Bottomonium and exotic spectroscopy

R. Garg on behalf of the Belle II Collaboration[1,*,**]

[1]Carnegie Mellon University, 5000 Forbes Avenue, Pittsburgh, USA

Abstract. This proceedings summarize the most recent measurements of exotic bottomonium states to probe the fundamentals of QCD at the Belle, Belle II and LHCb experiments.

1 Introduction

Bottomonium spectroscopy offers multiple opportunities to investigate the non-perturbative behavior of quantum chromodynamics. In recent years, bottomonium spectroscopy has shown a number of unexpected results. These include the observation of the spin-singlet P-wave state, $h_b(2P)$, and several unexpected exotic bottomoinum-like states, labeled X, Y, and Z states. Since these exotic hadrons are not predicted by the quark model, different compositions are being considered, such as compact tetraquarks, mesonic molecules, and hybrids. More experimental results are needed in this sector to better understand the phenomenology of bottomonium(-like) states and their transitions.

2 Recent bottomonium results from the Belle Collaboration

The spin-singlet P-wave state $h_b(2P)$ is observed by the Belle Collaboration [1] at a surprisingly high rate. The production of $b\bar{b}$ spin singlets is generally rare in e^+e^- collisions because it requires the spin flip of a heavy quark in a hadronic or radiative transition. In this section, we discuss the studies performed on $h_b(2P)$ decays by the Belle Collaboration.

2.1 Evidence of $h_b(2P) \to \Upsilon(1S)\,\eta$ decay and search for $h_b(1P, 2P) \to \Upsilon(1S)\,\pi^0$

The $h_b(1P, 2P)$ hadronic transitions to the $\Upsilon(1S)$ state with emission of η or π^0 are studied using a sample of 121.4 fb^{-1} data and 12.0 fb^{-1} of energy-scan data collected at and near $\Upsilon(5S)$, respectively [2].

The decay $h_b(2P) \to \Upsilon(1S)\,\eta$ is suppressed by heavy quark spin symmetry. The decay properties of the spin-singlet $^1P_1$ states, $h_b(1P)$ and $h_b(2P)$ [1] are expected to be similar to those of their spin-triplet partners, $\chi_{b1}(1P)$ and $\chi_{b1}(2P)$ [3]. Theoretically, it is predicted that the ratio, R_{h_b}, of the annihilation rates for $h_b(2P)$ and $h_b(1P)$ is the same as the corresponding ratio, $R_{\chi_{b1}}$, for $\chi_{b1}(2P)$ and $\chi_{b1}(1P)$ [4]. The measured value of $R_{h_b}/R_{\chi_{b1}}$ based on current branching fractions is $0.24^{+0.47}_{-0.24}$, which is 1.5 σ away from the expected value of 1. However, this discrepancy would increase further if the rate of $h_b(2P) \to \Upsilon(1S)\,\eta$ is measured and included [4].

*e-mail: renu2@andrew.cmu.edu

**Supported by U. S. Dept. of Energy under contract number DE-SC-0010118

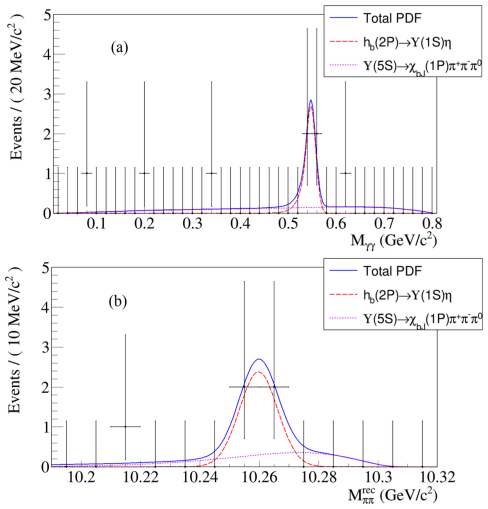

Figure 1. Comparison of 2–D fit projections of $M_{\gamma\gamma}$ in the signal region of $10.242 < M^{\rm rec}_{\pi\pi} < 10.278$ GeV/c^2 (top) and $M^{\rm rec}_{\pi\pi}$ in the signal region of $450 < M_{\gamma\gamma} < 600$ MeV/c^2 (bottom) for $h_b(2P) \to \Upsilon(1S)\,\eta$ decay mode. The solid lines and points with error bars represent the fit results and the data, respectively.

Evidence for the $h_b(2P) \to \Upsilon(1S)\,\eta$ transition is found with 3.5σ signal significance, and the measured branching fraction is $\mathcal{B}(h_b(2P) \to \Upsilon(1S)\,\eta) = (7.1^{+3.5}_{-3.2} \pm 0.8) \times 10^{-3}$. Figure 1 displays the diphoton invariant mass, $M_{\gamma\gamma}$, and the dipion recoil mass, $M^{\rm rec}_{\pi\pi}$, for decay $h_b(2P) \to \Upsilon(1S)\,\eta$. In absence of a significant signal for the $h_b(1P, 2P) \to \Upsilon(1S)\,\pi^0$ decay mode, the upper limits on their branching fractions, $h_b(1P) \to \Upsilon(1S)\,\pi^0 < 1.8 \times 10^{-3}$ and $h_b(2P) \to \Upsilon(1S)\,\pi^0 < 1.8 \times 10^{-3}$ at the 90% confidence level are set.

2.2 Search for $h_b(2P) \to \gamma\chi_{bJ}(1P)$ at $\sqrt{s}$ = 10.860 GeV

The transitions between the spin-singlet state and spin-triplet states, $h_b(2P) \to \gamma\chi_{bJ}(1P)$, are reported using a data sample of 121.4 fb^{-1} obtained at $\sqrt{s}$ = 10.860 GeV [5]. According to the Relativized Quark Model [6], these transitions are expected to be suppressed due to the heavy-quark spin flip, and branching fractions are predicted to be of the order $10^{-6} - 10^{-5}$. However, considering coupled channel effects [7] increases the predicted branching fractions for these transitions to the order $10^{-2} - 10^{-1}$. Experimental results are needed to assess the importance of these effects in the transitions.

Channel	Branching fraction ($\mathcal{B}$)
$h_b(2P) \to \gamma\chi_{b2}(1P)$	$< 1.2 \times 10^{-2}$
$h_b(2P) \to \gamma\chi_{b1}(1P)$	$< 5.4 \times 10^{-3}$
$h_b(2P) \to \gamma\chi_{b0}(1P)$	$< 2.7 \times 10^{-1}$

Table 1. Observed upper limits at 90% CL for the branching fractions.

No significant signal for $h_b(2P) \to \gamma\chi_{bJ}(1P)$ is observed. Therefore, the upper limits on their branching fractions are set; see Table 1. The comparison of experimental upper limits

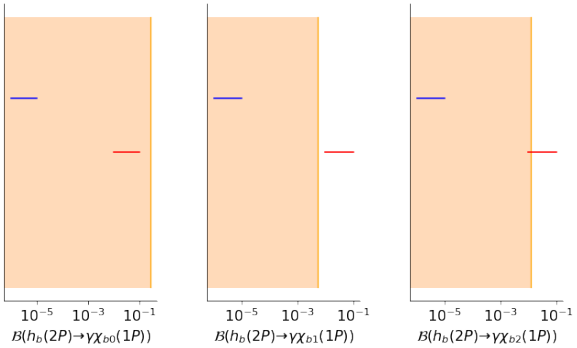

Figure 2. Comparison of experimental allowed regions of branching fractions (orange shaded area), and the relativized quark model (blue) and coupled channel model (red) predictions.

and theoretical predictions is shown in Fig. 2. The upper limit on the $\chi_{bJ}(1P)$ channel is consistent with the expectations of the relativized quark model [6] but the $\chi_{b1}(1P)$ excludes the results of the coupled channel model [7].

3 Recent bottomonium results from the Belle II Collaboration

The $\Upsilon(10753)$ bottomonium-like vector state was observed in the cross-section for the process of $e^+e^- \to \pi^+\pi^-\,\Upsilon(nS)$ (n = 1, 2, 3) by Belle [8] and in fits to the $e^+e^- \to b\bar{b}$ cross-sections at energies $\sqrt{s}$ from 10.52 to 11.02 GeV [9]. The mass and width of this state are $M = (10753 \pm 6)$ MeV/c^2 and $\Gamma = (36^{+18}_{-12})$ MeV. The mass of this state is not consistent with any predicted states. So it is difficult to assign $\Upsilon(10753)$ as a conventional bottomoium state. The unexpected presence of this state has provoked theoretical interest. The most popular interpretation of the $\Upsilon(10753)$ is a mixture of $\Upsilon(4S)$ and $\Upsilon(3D)$ states [10, 11]. There are several other interpretations, such as conventional bottomonium [12–17], a hybrid [18], a hadronic molecule with a small admixture of bottomonium [19], or a tetraquark state [20, 21]. However, so far there has been no conclusive explanation.

Measurements of the properties and decay modes of $\Upsilon(10753)$ are important to understand its nature. Therefore, Belle II performed an energy scan in the vicinity of the $\Upsilon(10753)$, collecting 19.3 fb^{-1} at the four center-of-mass (c.m.) energy points $\sqrt{s}$ = 10.653, 10.701, 10.745, 10.805 GeV, to confirm the existence of this new state and study its properties.

3.1 Study of $\Upsilon(10753) \to \pi^+\pi^-\pi^0\,\gamma\,\Upsilon(1S)$

One interpretation of the $\Upsilon(10753)$ as an admixture of $\Upsilon(4S)$ and $\Upsilon(3D)$ states predicts that branching fractions for $\Upsilon(10753) \to \omega\,\chi_{bJ}$, $\chi_{bJ} \to \gamma\,\Upsilon(1S)$ [14] and $\Upsilon(10753) \to \pi^+\pi^-\,\Upsilon(nS)$ [15] are comparable and of order 10^{-3}. In addition, the branching fraction ratio for $\Upsilon(10753) \to \omega\,\chi_{b1}$ and $\Upsilon(10753) \to \omega\,\chi_{b2}$ is expected to be about 0.2 [14]. The process $\Upsilon(10753) \to \gamma X_b$, $X_b \to \omega\Upsilon(1S)$, which shares the same final states as $\Upsilon(10753) \to \omega\,\chi_{bJ}$, provides access to the X_b. The X_b is the bottomonium analogue of the $X(3872)$. Its existence has been predicted in molecular [22–24] and tetraquark models [25–27].

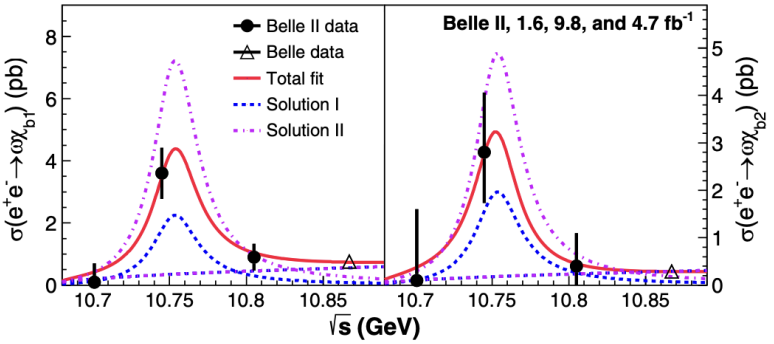

Figure 3. Energy dependence of the Born cross sections for $e^+e^- \to \omega\,\chi_{b1}$ (left) and $e^+e^- \to \omega\,\chi_{b2}$ (right). Circles and triangles show results from this work and Belle experiment, respectively. Error bars represent combined statistical and systematic uncertainties. Curves show the fit results and various components of the fit function, where the two solutions correspond to the two signs of interference.

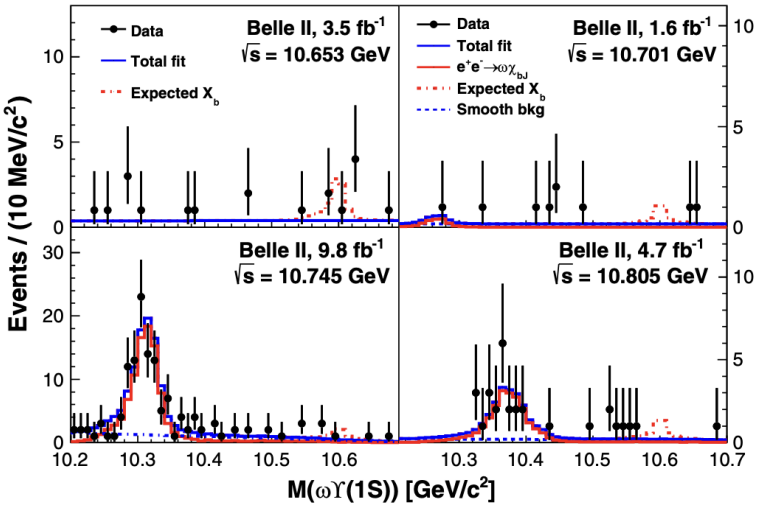

Figure 4. Distributions of $\omega\Upsilon(1S)$ mass from data at $\sqrt{s}$ = 10.653, 10.701, 10.745, and 10.805 GeV. The red dash-dotted histograms are from simulated events $\Upsilon(10753) \to \gamma X_b$, $X_b \to \omega\Upsilon(1S)$ with the X_b mass fixed at 10.6 GeV/c^2 and yields fixed at the upper limit values. The red soild lines are the reflections of the $e^+e^- \to \omega\,\chi_{bJ}$ signals.

A significant signal for $e^+e^- \to \omega\,\chi_{b1}$ and evidence for the $e^+e^- \to \omega\,\chi_{b2}$ process at $\sqrt{s}$ = 10.745 GeV are found [29]. The corresponding Born cross-sections (σ) are calculated using

$$\sigma(e^+e^- \to \omega\,\chi_{bJ}) = \frac{N\ |1-\Pi|^2}{\mathcal{L}\,\varepsilon\,\mathcal{B}_{\rm int}\ (1+\delta_{\rm ISR})}$$

where, N, $\mathcal{L}$, ε, $\mathcal{B}_{\rm int}$, $|1-\Pi|^2$, and $(1+\delta_{\rm ISR})$ are the yield of a specific decay mode, the integrated luminosity, the reconstruction efficiency, the product of the branching fractions of

the intermediate states, the vacuum polarization factor, and the radiative-correction factor, respectively. The Born cross sections measured at $\sqrt{s} = 10.745$ GeV for the process $e^+e^- \to \omega\chi_{b1}$ and $e^+e^- \to \omega\chi_{b2}$ are $(3.6 \pm 0.7 \pm 0.5)$ pb and $(2.8^{+1.2}_{-1.0} \pm 0.4)$ pb, respectively, and are shown in Fig. 3 as a function of $\sqrt{s}$.

The ratio, $\sigma_B(e^+e^- \to \omega\chi_{b1})/\sigma_B(e^+e^- \to \omega\chi_{b2}) = 1.3 \pm 0.6$ at $\sqrt{s} = 10.745$ GeV is also measured, where statistical and systematic uncertainties are included. This observed ratio contradicts the expectation of 15 for a pure D-wave bottomonium state [28], and there is also a 1.8σ difference from the prediction of 0.2 for a $S - D$ mixed state [14].

The distributions of $M_{\omega\Upsilon(1S)}$ within $0.70 < M_{\pi^+\pi^-\pi^0} < 0.86$ GeV/c^2 at $\sqrt{s} = 10.653$, 10.701, 10.745, and 10.805 GeV are shown in Fig. 4. Reflections of the $e^+e^- \to \omega\chi_{bJ}$ signals are observed, but no evidence of a X_b signal is obtained for X_b masses between 10.45 and 10.65 GeV/c^2. Thus, the upper limits at 90% Bayesian confidence on the products of Born cross section for $e^+e^- \to \gamma X_b$ and branching fraction for $X_b \to \omega\Upsilon(1S)$ are set to be 0.55, 0.84, 0.14, and 0.37 pb at 10.653, 10.701, 10.745, and 10.805 GeV, respectively.

3.2 Study of $\Upsilon(10753) \to \omega\chi_{b0}(1P)/\omega\eta_b(1S)$

The processes $e^+e^- \to \omega\eta_b(1S)$ and $e^+e^- \to \omega\chi_{b0}(1P)$ are also studied at a $\sqrt{s} = 10.745$ GeV [31]. Theoretically, in the tetraquark model [20], the decay rate of $\Upsilon(10753) \to \omega\eta_b(1S)$ should be strongly enhanced compared to the decay rates of $\Upsilon(10753) \to \pi^+\pi^-\Upsilon(nS)$. However, the $4S-3D$ mixing model predicts that the decay rate of $\Upsilon(10753) \to \omega\eta_b(1S)$ is lower than the decay rate of $\Upsilon(10753) \to \pi^+\pi^-\Upsilon(nS)$ by a factor $0.2 - 0.4$ [32]. Therefore, experimental results are desirable.

The $\eta_b(1S)$ and $\chi_{b0}(1P)$ mesons do not have exclusive decay channels with a large product of efficiency and branching fraction. Thus, the partial reconstruction of an ω meson in the decay $\pi^+\pi^-\pi^0$ is done and the recoil mass,

$$M_{\rm recoil}(\pi^+\pi^-\pi^0) = \sqrt{\left(\frac{\sqrt{s}-E_\omega}{c^2}\right)^2 - \left(\frac{p_\omega}{c}\right)^2}$$

is used as the signal extraction variable, where E_ω and p_ω are the energy and momentum of the ω meson in the c.m. frame. In a previous study [29], the process $e^+e^- \to \omega\chi_{b0}(1P)$ using full reconstruction of the decay $\chi_{b0}(1P) \to \gamma\Upsilon(1S)$ was searched and no significant signal was found. The probability of the decay $\chi_{b0}(1P) \to \gamma\Upsilon(1S)$ is small; therefore, the sensitivity of partial reconstruction, applied in this analysis, might be higher than that of full reconstruction.

The fit results of $M_{\rm recoil}(\pi^+\pi^-\pi^0)$ for the decays $e^+e^- \to \omega\eta_b(1S)$ and $e^+e^- \to \omega\chi_{b0}(1P)$ are shown in Fig. 5. No significant signals are observed. Therefore, the upper limits on the Born-level cross sections are set at 90% confidence level:

$$\sigma_B(e^+e^- \to \omega\eta_b(1S)) < 2.5 \text{ pb},$$

$$\sigma_B(e^+e^- \to \omega\chi_{b0}(1P)) < 8.7 \text{ pb}.$$

The upper limit on the $e^+e^- \to \omega\chi_{b0}(1P)$ cross section is comparable to the upper limit of 11.3 pb obtained by using a full reconstruction [29]. The upper limit obtained in $\sigma_B(e^+e^- \to \omega\eta_b(1S))$ is close to the measured values of $\sigma_B(e^+e^- \to \pi^+\pi^-\Upsilon(nS))$, which are in the range $(1-3)$ pb [8]. Thus, results of this work do not support the prediction of the tetraquark model that the decay $\Upsilon(10753) \to \omega\eta_b(1S)$ is enhanced [20]. On the other hand, an upper limit of this work does not contradict the expectation of the $4S - 3D$ model.

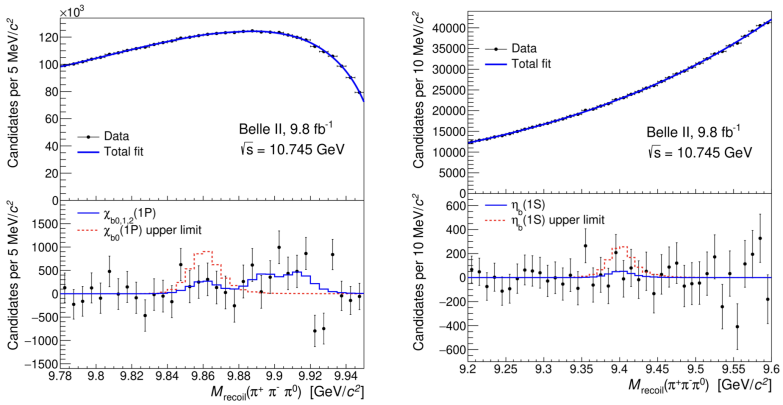

Figure 5. Distribution of $M_{\rm recoil}(\pi^+\pi^-\pi^0)$ for the $e^+e^- \to \omega\,\eta_b(1S)$ (left) and $e^+e^- \to \omega\,\chi_{b0}(1P)$ (right) candidates. The top distributions show data points with the fit function overlaid, and the bottom shows the data with the background component of the fit function subtracted. The solid histogram shows the fit function for the best fit; the dashed histogram shows the same function with the $J = 0$ yield fixed to the upper limit and $J = 1, 2$ yield set to 0.

The upper limit on the $\omega\,\chi_{b0}(1P)$ cross section is higher than the measured $\omega\,\chi_{b1}(1P)$ and $\omega\,\chi_{b2}(1P)$ cross sections of (3.6 ± 0.9) pb and (2.8 ± 1.3) pb, respectively [29]. For a mixed state $4S - 3D$, the decay rate of $\omega\,\chi_{b0}(1P)$ is expected to be comparable to the decay rates of $\omega\,\chi_{b1}(1P)$ and $\omega\,\chi_{b2}(1P)$ [15]; the measured upper limit of this work is consistent with this expectation.

3.3 Study of $\Upsilon(10753) \to \pi^+\pi^-\,\Upsilon(nS)$

An analysis of $\Upsilon(10753) \to \pi^+\pi^-\,\Upsilon(nS)$, where $n = 1, 2, 3$, using large data samples collected by the Belle II experiment is reported [33]. The final state $\pi^+\pi^-\,\Upsilon(nS)$ is reconstructed to form the $\Upsilon(10753)$, with the $\Upsilon(nS)$ decaying to a $\mu^+\mu^-$ pair, at $\sqrt{s}$ from 10.6 – 10.8 GeV. The fit to Born cross sections, σ_B, is performed for these processes as a function of $\sqrt{s}$ to measure the mass and width of $\Upsilon(10753)$. The intermediate states are also searched to study the dynamics of internal decay, e.g. $e^+e^- \to f_0(980)[\to \pi^+\pi^-]\Upsilon(nS)$ and exotic states, $e^+e^- \to \pi^\mp Z_b(10610, 10650)^\pm[\to \pi^\pm\,\Upsilon(nS)]$, which may provide deeper knowledge about the possible unconventional nature of the $\Upsilon(10753)$.

The Born cross sections as a function of energy are shown in Fig. 6. The signals for $\pi^+\pi^-\,\Upsilon(1S)$ and $\pi^+\pi^-\,\Upsilon(2S)$ are observed with greater than 8σ significance, while there is no evidence for $\pi^+\pi^-\,\Upsilon(3S)$.

The cross-section ratios $\sigma(\pi^+\pi^-\,\Upsilon(1S, 3S))/\sigma(\pi^+\pi^-\,\Upsilon(2S))$ at the resonance peak of the $\Upsilon(10753)$ are determined for the first time. They are $0.46^{+0.15}_{-0.12}$ and $0.10^{+0.05}_{-0.04}$ for $\pi^+\pi^-\Upsilon(1S)$ and $\pi^+\pi^-\,\Upsilon(3S)$, respectively. The ratio for $\pi^+\pi^-\,\Upsilon(1S)$ at the $\Upsilon(10753)$ peak is compatible with the ratios at the $\Upsilon(5S)$ and $\Upsilon(6S)$ peaks. However, the relative ratio of $\pi^+\pi^-\,\Upsilon(3S)$ at the $\Upsilon(10753)$ peak is about 3 – 4 times smaller than at the $\Upsilon(5S)$ and $\Upsilon(6S)$ peaks.

The distributions of the dipion mass, $M_{\pi^+\pi^-}$, and the maximal difference between the $\pi^+\pi^-\mu^+\mu^-$ mass and the $\pi^\pm\mu^+\mu^-$ mass, ΔM_π, in the signal regions are shown in Fig. 7. No evidence is found for these transitions occuring via the intermediate states $Z_b(10610, 10650)^\pm$. The dipion-invariant mass in $\pi^+\pi^-\,\Upsilon(1S)$ (Fig. 7, topleft) is consistent with the simulated

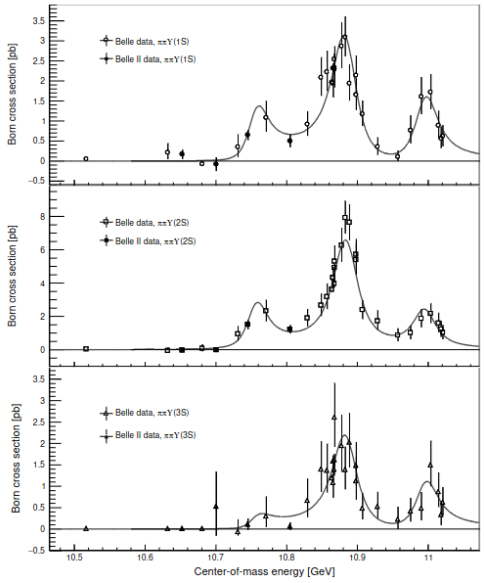

Figure 6. Born cross sections for $\pi^+\pi^-\,\Upsilon(1S)$ (top), $\pi^+\pi^-\,\Upsilon(2S)$ (middle), and $\pi^+\pi^-\,\Upsilon(3S)$ (bottom), with fit results overlaid.

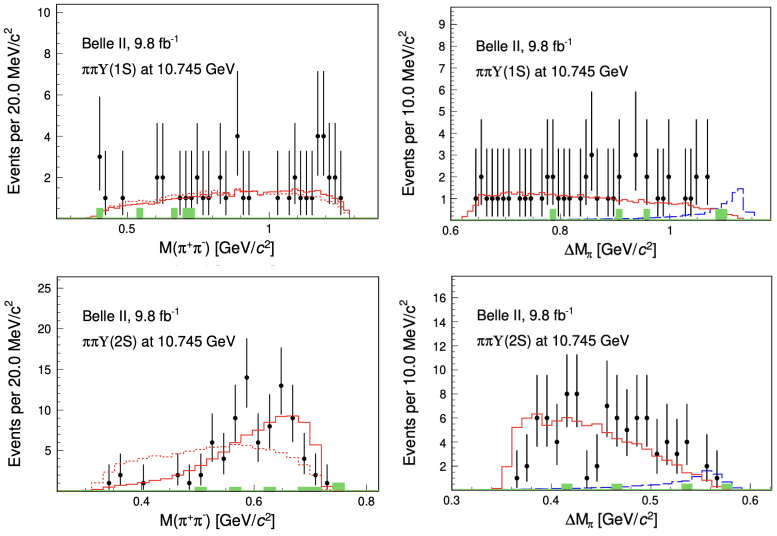

Figure 7. Distributions of dipion mass (left) and maximal difference between the $\pi^+\pi^-\mu^+\mu^-$ mass and the $\pi^\pm\mu^+\mu^-$ mass (right) for $\pi^+\pi^-\,\Upsilon(1S)$ (top) and $\pi^+\pi^-\,\Upsilon(2S)$ (bottom) at $\sqrt{s} = 10.745$ GeV. Points with error bars, green shaded histograms, red histograms, red dotted histogram, and blue dashed histogram show the events in the signal region from data, events in the sideband region, weighted simulated signal, phase space signal MC simulation, and $Z_b(10610, 10650)^\pm$ from MC simulation, respectively.

phase-space distribution. The dipion-invariant mass in the production of $\pi^+\pi^-\,\Upsilon(2S)$ (Fig. 7, bottom left) is similar to that observed in the $\Upsilon(2S) \to \pi^+\pi^-\,\Upsilon(1S)$ process.

The mass and width of the $\Upsilon(10753)$ are measured as $(10756.3 \pm 2.7 \pm 0.6)$ MeV/c^2 and $(29.7 \pm 8.5 \pm 1.1)$ MeV, respectively, which are consistent with previous measurements but with uncertainties nearly a factor of two smaller. These results supersede the previous Belle result [8]. This improvement in accuracy provides a more precise comparison for theoretical calculations.

3.4 Energy dependence of $e^+e^- \to B^{(*)}\bar{B}^{(*)}$ cross-section

The $B^{(*)}\bar{B}^{(*)}$ final states are expected to be the main hadronization states for $b\bar{b}$ pairs and be the most significant contribution to the total $b\bar{b}$ cross-section. Measuring the $e^+e^- \to B^{(*)}\bar{B}^{(*)}$ cross sections provides important information on the structure of bottomonium(-like) resonances. These measured cross sections can be used in the coupled channel analysis to extract the parameters of the $b\bar{b}$ states. The analysis follows the analogous measurement made at Belle [35], where the measured energy dependencies of $\sigma(e^+e^- \to B^{(*)}\bar{B}^{(*)})$ showed oscillatory behavior.

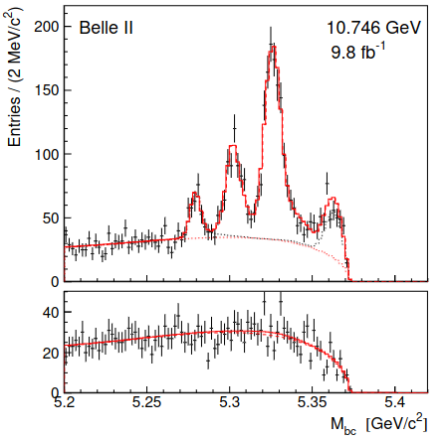

Figure 8. Distribution of $M_{\rm bc}$ at $\sqrt{s} = 10.746$ GeV. The top panel corresponds to the signal region, and the bottom to the sideband. The red solid and dashed histogram show the result of the fit and the smooth background. The black dotted histogram shows the sum of the smooth background and the $B\bar{B}$ channel, which includes a peak near the threshold due to the ISR production of $\Upsilon(4S)$.

The measurement of the energy dependence of the $e^+e^- \to B\bar{B}$, $e^+e^- \to B\bar{B}^*$, and $e^+e^- \to B^*\bar{B}^*$ exclusive cross sections is reported [34]. A full reconstruction of one B meson is performed in hadronic channels and identify the $B\bar{B}$, $B\bar{B}^*$, and $B^*\bar{B}^*$ signals using the $M_{\rm bc}$ distribution, $M_{\rm bc} = \sqrt{(E_{cm}/2)^2 - p_B^2}$, where E_{cm} and p_B are the c.m. energy and B-candidate momentum measured in the c.m. frame, respectively. The $M_{\rm bc}$ distribution for the $B\bar{B}$ events peaks at the nominal B-meson mass, m_B, while the distributions for the $B\bar{B}^*$ and $B^*\bar{B}^*$ events peak approximately at $m_B - \Delta m_{B^*}/2$ and $m_B - \Delta m_{B^*}$, respectively, where Δm_{B^*} is the mass difference of the B^* and B mesons. The distribution of $M_{\rm bc}$ obtained at $\sqrt{s} = 10.746$ GeV is shown in Fig. 8.

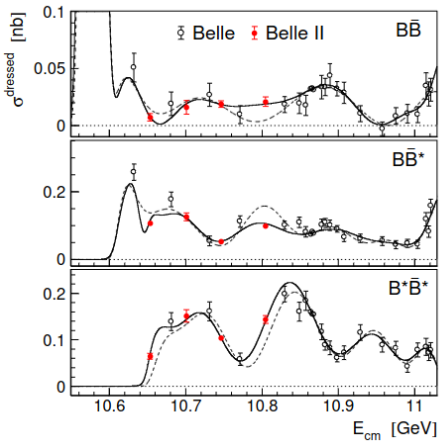

Figure 9. The energy dependence of the $e^+e^- \to B\bar{B}$ (top), $e^+e^- \to B\bar{B}^*$ (middle), and $e^+e^- \to B^*\bar{B}^*$ (bottom) Born cross-section. Red and black circles show the Belle II and Belle results. The solid and dashed curves show the fit results to Belle + Belle II points and Belle points, respectively.

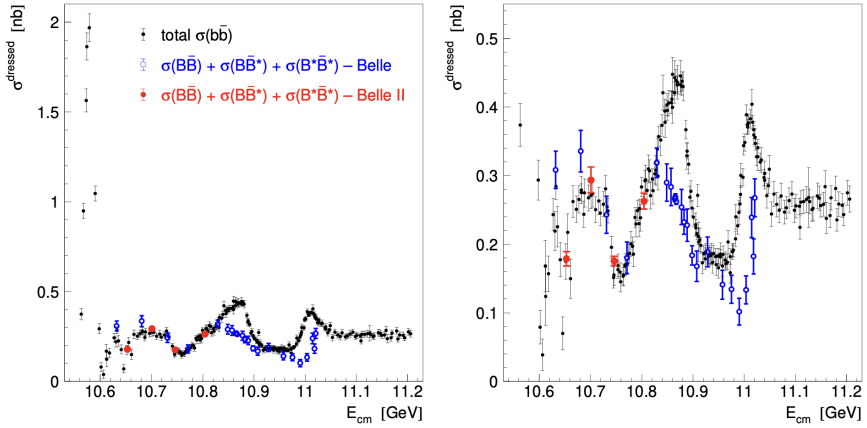

Figure 10. Energy dependence of the total $b\bar{b}$ dressed cross-section obtained in Ref. [9] from the visible cross-sections measured by Belle [37], and BaBar [36] (black circles) and the sum of the exclusive $B\bar{B}$, $B\bar{B}^*$, and $B^*\bar{B}^*$ cross-sections measured by Belle [35] (open blue circles) and in this work (filled red circles). The right panel shows the low cross-section region with an expanded scale.

The signal yields are estimated by fitting the $M_{\rm bc}$ distributions. The dressed cross-section is calculated as

$$\sigma^{\rm dressed} = \frac{N}{(1+\delta_{ISR})\ \mathcal{L}\,\varepsilon}$$

where, N, $(1+\delta_{ISR})$, $\mathcal{L}$ and ε are the yield of a specific decay mode, the radiative correction factor, the integrated luminosity and the reconstruction efficiency, respectively. A simultaneous fit of the energy dependence of the $e^+e^- \to B\bar{B}$, $e^+e^- \to B\bar{B}^*$, and $e^+e^- \to B^*\bar{B}^*$ cross sections and of the total $e^+e^- \to b\bar{b}$ cross section is performed. The results are shown in Fig. 9, where the previous Belle measurements are included.

Figure 10 shows the sum of the exclusive $B\bar{B}$, $B\bar{B}^*$, and $B^*\bar{B}^*$ cross-sections measured in this work and in the Belle experiment [35], superimposed on the total $b\bar{b}$ dressed cross-section [9]. The sum of measurements performed in this work agrees well with the total cross-section at low energy. The deviation at higher energy is presumably due to the contribution of B_s^0 mesons, multibody final states $B^{(*)}\bar{B}^{(*)}\pi(\pi)$, and production of bottomonia in association with light hadrons.

4 Recent bottomonium results from the LHCb Collaboration

Hadroproduction of heavy quarkonia has been extensively studied to probe quantum chromodynamics (QCD) [38]. A pair of heavy quarkonia can be produced through either single-parton scattering (SPS), or double-parton scattering (DPS) in hadron collisions.

The production of $J/\psi-\Upsilon$ in $p\bar{p}$ collisions is studied at a c.m. energy of $\sqrt{s} = 13$ TeV [39]. The J/ψ and Υ mesons are reconstructed in the dimuon final state. The DPS cross-section, $\sigma_{\rm DPS}(J/\psi - \Upsilon)$, can be estimated from the J/ψ and Υ cross-sections, $\sigma(J/\psi)$ and $\sigma(\Upsilon)$, as

$$\sigma_{\rm DPS}(J/\psi - \Upsilon) = \frac{\sigma(J/\psi) \times \sigma(\Upsilon)}{\sigma_{\rm eff}}$$

where $\sigma_{\rm eff}$ is the effective cross section parameter. This effective cross section is expected to be universal, based on the assumptions that the two sets of colliding partons are uncorrelated and that the longitudinal and transverse components of the parton distribution function factorize. The invariant mass distributions of the candidates J/ψ and Υ, together with the fit

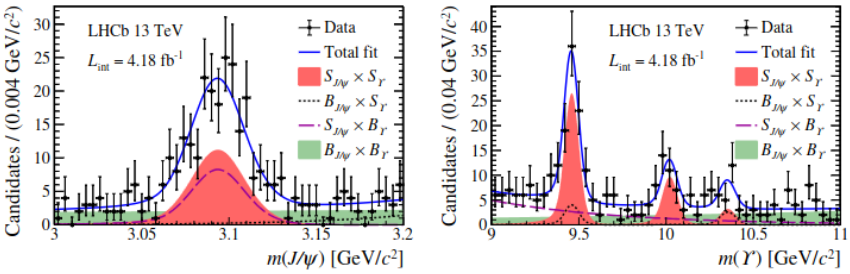

Figure 11. Two dimensional fit projections for $M_{J/\psi}$ (left) and M_Υ (right). The black points with error bars, blue solid line and red shaded area represent the data, the result of the fit to the data sample and the signal component, respectively. The black (dotted), violet (dashed) lines and green shaded area represent the background where one dimuon candidate is a true meson decay, the other is combinatorial background and the background where both the J/ψ and Υ candidates are combinatorial background, respectively.

projections, are shown in Fig. 11.

A significant signal for $J/\psi - \Upsilon(1S)$ production is observed with a significance of 7.9σ, and evidence is found for $J/\psi - \Upsilon(2S)$ production. The cross sections for $J/\psi - \Upsilon(1S)$ and $J/\psi - \Upsilon(2S)$ production are measured as 133 ± 22 (stat) ± 7 (syst) ± 3 ($\mathcal{B}$) pb and 76 ± 21 (stat) $\pm$ 4 (syst) ± 7 ($\mathcal{B}$) pb, respectively. The effective cross sections for $J/\psi - \Upsilon(1S)$ and $J/\psi - \Upsilon(2S)$ production are also measured:

$$\sigma_{\rm eff}(J/\psi - \Upsilon(1S)) = 26 \pm 5 \pm 2^{+22}_{-3}\ \text{mb},$$

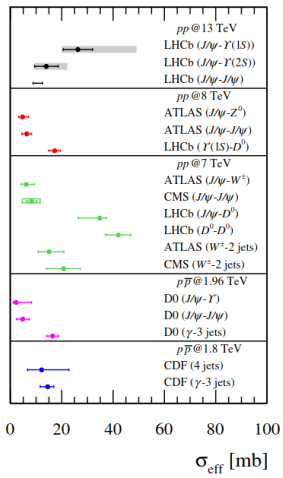

Figure 12. Effective cross sections measured in different particle production by various experiments.

$$\sigma_{\rm eff}(J/\psi - \Upsilon(2S)) = 14 \pm 5 \pm 1^{+7}_{-1}\ {\rm mb}$$

where the first, second and third uncertainties are statistical, systematic, and theoretical, respectively. The effective cross sections for $J/\psi - \Upsilon(1S)$ and $J/\psi - \Upsilon(2S)$ production are consistent with measurements using hadroproduction of other particles, as shown in Fig. 12.

5 Summary

The current understanding of the physics of highly excited heavy bottomonium is incomplete. In this proceeding, we have shown recent measurements performed by the Belle, Belle II and LHCb Collaborations. These results are of great importance in understanding the nature of the bottomonium(-like) states above the open flavor threshold. The present status of the $\Upsilon(10753)$ is shown in Fig. 13. The unique data set collected at center-of-mass energies around 10.75 GeV will enable Belle II to provide further exciting results in the bottomonuim sector in the

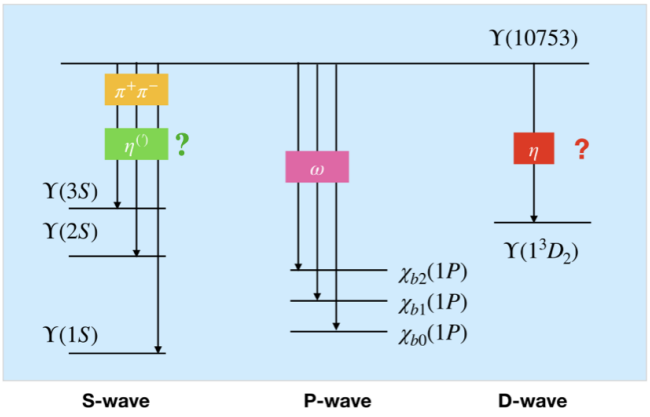

Figure 13. Present status of $\Upsilon(10753)$ state.

near future. LHCb results on effective cross-sections of $J/\psi - \Upsilon$ production are consistent with other particle productions measurements.

References

[1] I. Adachi *et al.* (Belle Collaboration), Phys. Rev. Lett. **108** (2012) 032001.
[2] E. Kovalenko *et al.* (Belle Collaboration), arXiv:2407.03783.
[3] S. Godfrey and J. L. Rosner, Phys. Rev. D **66** (2002) 014012.
[4] X. Li and M. B. Voloshin, Phys. Rev. D **86** (2012) 094013.
[5] Preliminary results.
[6] S. Godfrey and N. Isgur, Phys. Rev. D **32** (1985) 189383.
[7] F.-K. Guo, U.-G. Meißner, and Z. Yang, Phys. Lett. B **760** (2016) 417387.
[8] R. Mizuk *et al.* (Belle Collaboration), J. High Energy Phys. **10** (2019) 220.
[9] X. K. Dong, X. H. Mo, P. Wang, and C. Z. Yuan, Chin. Phys. C **44** (2020) 083001.
[10] J. F. Giron and R. F. Lebed, Phys. Rev. D **102** (2020) 014036.
[11] B. Chen, A. L. Zhang, and J. He, Phys. Rev. D **101** (2020) 014020.
[12] Q. Li, M. S. Liu, Q. F. Lü, L. C. Gui, and X. H. Zhong, Eur. Phys. J. C **80** (2020) 59.
[13] W. H. Liang, N. Ikeno, and E. Oset, Phys. Lett. B **803** (2020) 135340.
[14] Y. S. Li, Z. Y. Bai, Q. Huang, and X. Liu, Phys. Rev. D **104** (2021) 034036.
[15] Z. Y. Bai, Y. S. Li, Q. Huang, X. Liu, and T. Matsuki, Phys. Rev. D **105** (2022) 074007.
[16] N. Hüsken, R. E. Mitchell, and E. S. Swanson, Phys. Rev. D **106** (2022) 094013.
[17] V. Kher, R. Chaturvedi, N. Devlani, and A. K. Rai, Eur. Phys. J. Plus **137** (2022) 357.
[18] N. Brambilla, W. K. Lai, J. Segovia, J. T. Castellà, and A. Vairo, Phys. Rev. D **99** (2019) 014017.
[19] P. Bicudo, N. Cardoso, L. Müller, and M. Wagner, Phys. Rev. D **103** (2021) 074507.
[20] Z. G. Wang, Chin. Phys. C **43** (2019) 123102.
[21] A. Ali, L. Maiani, A. Y. Parkhomenko, and W. Wang, Phys. Lett. B **802** (2020) 135217.
[22] N. A. Tornqvist, Z. Phys. C **61** (1994) 525.
[23] F. K. Guo, C. H. Duque, J. Nieves, and M. P. Valderrama, Phys. Rev. D **88** (2013) 054007.
[24] M. Karliner and S. Nussinov, J. High Energy Phys. **07** (2013) 153.
[25] D. Ebert, R. N. Faustov, and V. O. Galkin, Phys. Lett. B **634** (2006) 214.
[26] D. Ebert, R. N. Faustov, and V. O. Galkin, Mod. Phys. Lett. **24A** (2009) 567.
[27] A. Ali, C. Hambrock, I. Ahmed, and M. J. Aslam, Phys. Lett. B **684** (2010) 28.
[28] F. K. Guo, Ulf-G. Meißner, and C. P. Shen, Phys. Lett. B **738** (2014) 172.
[29] I. Adachi *et al.* (Belle II Collaboration), Phys. Rev. Lett. **130** (2023) 091902.
[30] X. H. He *et al.* (Belle Collaboration), Phys. Rev. Lett. **113** (2014) 142001.
[31] I. Adachi *et al.* (Belle II Collaboration), Phys. Rev. D **109** (2024) 072013.
[32] S. Liu, Z. Cai, Z. Jia, G. Li and J. Xie, arXiv:2312.02761563.
[33] I. Adachi *et al.* (Belle II Collaboration), arXiv:2401.12021v3.
[34] I. Adachi *et al.* (Belle II Collaboration), arXiv:2405.18928v1.
[35] R. Mizuk *et al.* (Belle Collaboration), J. High Energy Phys. **06** (2021) 137.
[36] B. Aubert *et al.* (BaBar Collaboration), Phys. Rev. Lett. **102** (2009) 012001.
[37] D. Santel *et al.* (Belle Collaboration), Phys. Rev. D **93** (2016) 011101.
[38] E. Chapon *et al.* (LHCb Collaboration), Prog. Part. Nucl. Phys. **122** (2022) 103906.
[39] R. Aaij *et al.* (LHCb Collaboration), J. High Energy Phys. **08** (2023) 093.